Mixing in a swarm of bubbles rising in a confined cell measured by mean of PLIF with two different dyes

Emmanuella Bouche · Sébastien Cazin · Véronique Roig · Frédéric Risso

Abstract The present contribution reports an experimental study of the mixing of a passive scalar of very low diffusivity in a homogeneous swarm of inertial bubbles rising in a thin gap. A patch of fluorescent dye is injected within the swarm, and we observe the evolution of its mass in a given region of observation. We analyse the effect of the liquid agitation on the mixing mechanisms varying the gas volume fraction from 1.3 to 7.5 %, while the Reynolds number of the bubbles, $Re = 450$, their Weber number, $We = 0.7$, and the gap-to-bubble diameter ratio, $w/d = 0.25$, are kept approximately constant. Here, the in-plane local mass of dye is measured by using a two-dyes planar laser-induced fluorescence (PLIF) technique that has been adapted to fix the problem of multiple light reflections at the bubble interfaces. Indeed, they induce both temporal and spatial variations of the captured light intensity that are superimposed to the effective fluorescence signal and prevent from using a standard PLIF technique. The analysis of the instantaneous concentration fields reveals the dominant role of the bubble wakes in the scalar transport. It is shown that mixing in this planar confined geometry is very efficient and enhanced by the increasing gas volume fraction. The present study also highlights that the mixing is not governed by a Fickian law of diffusion.

E. Bouche (✉) · S. Cazin · V. Roig · F. Risso
Institut de Mécanique des Fluides de Toulouse, Université de Toulouse (INPT, UPS) and CNRS, Allée C. Soula, 31400 Toulouse, France
e-mail: emmanuella.bouche@coria.fr

E. Bouche · S. Cazin · V. Roig · F. Risso
Fédération de Recherche FERMaT, CNRS, Allée C. Soula, 31400 Toulouse, France

Present Address:
E. Bouche
CNRS UMR 6614 CORIA, Université et INSA de Rouen, Avenue de l'Université, 76801 Saint Etienne du Rouvray, France

1 Introduction

A lot of chemical reactors or heat exchangers consist of bubble columns. In order to improve the efficiency of industrial processes, it is important to optimize mass or heat transfers through gas–liquid interfaces as well as mixing in the liquid phase in such systems. However, little is known about mixing in bubbly flows. As an example, we are still unable to predict the time needed to disperse a dye in a homogeneous swarm of bubbles rising in a liquid at rest. Local mechanisms responsible for mixing of a passive scalar by the disperse phase have been recently identified in a random array of fixed spheres mimicking a bubble swarm (Besnaci et al. 2010). The first mechanism is the distortion of the dye by direct interactions with the spheres: a dye filament is observed to be elongated, twisted or transformed into a sheet by the strong fluid deformations localized in the vicinity of the spheres. The other mechanism is the transport of dye by the turbulence that is generated by wake interactions. In a homogeneous swarm of high-Re rising bubbles, the mixing is also influenced by the relative motions of the bubbles. At large Reynolds number, the major ingredient controlling the mixing is the wake contribution. Theoretical models based on the potential flow approximation (Mareuge and Lance 1995; Eames and Bush 1998), which ignores the wakes, are thus not able to reproduce the great efficiency and anisotropy of the mixing observed in experimental bubbly flows (Mareuge and

Lance 1995; Abbas et al. 2009). To develop general models, it is relevant to investigate different flows where the relative weight of the various elementary mechanisms is changed. This is the reason why we explore the mixing in a confined swarm of bubbles rising at high Reynolds number within a Hele-Shaw cell. This allows changing the vortex dynamics as compared to 3D bubble swarms. Previous studies investigated the dynamics of both a single bubble (Roig et al. 2012) and of a homogeneous swarm of bubbles (Bouche et al. 2010, 2012) confined in a thin gap. For a Reynolds number of about 450, an isolated confined bubble rises along a sinusoidal path, keeping a constant elliptical shape and generating a velocity perturbation in the liquid similar to that of an unconfined 3D bubble, i.e. with a potential flow upstream and an unsteady wake with vortex shedding downstream. However, the wake is strongly attenuated by the shear stress at the wall and decreases exponentially with time. Its lifetime is related to the viscous time $\tau = w^2/\nu$, where w is the gap thickness and ν is the kinematic viscosity. In the swarm, as soon as the gas volume fraction is no longer negligible, hydrodynamic interactions start to play a role. The short bubble wakes and the vortex shedding generates liquid fluctuations that are mostly localized in the vicinity of the bubbles, the locations of which are statistically independent from each other. The agitation in the liquid phase thus results from wake interactions as in 3D bubble swarms, but turbulence can hardly develop in a confined geometry as vortices have a short lifetime of order τ (Bouche et al. 2010).

The present contribution reports an experimental study of the mixing of a passive fluorescent dye of very low molecular diffusivity in a homogeneous swarm of high Reynolds number bubbles ($Re = 450$) rising confined in a Hele-Shaw cell, and for various gas volume fractions. Here, the mixing of the dye is driven by the liquid agitation generated by the rising bubbles. A patch of fluorescent dye is first injected within the swarm. The evolution of the mass of dye is measured by means of planar laser-induced fluorescence (PLIF). This allows us to discuss the specific features of the mixing induced by confined bubbles. PLIF technique is now widely used to address scalar transport processes, as concentration or temperature (Crimaldi 2008). It has been shown to be significantly improved by the simultaneous use of several fluorescent tracers (Coppeta and Rogers 1998; Sakakibara and Adrian 1999; Soltys and Crimaldi 2011). In bubbly flows, PLIF has also already been used to investigate the gas–liquid mass transfer around a single bubble by using oxygen-quenching or pH-sensitive dye techniques (Roudet 2008; Stöhr et al. 2009; François et al. 2011). However, to our knowledge, very few studies have focused on concentration measurements in bubble swarms, even for a passive scalar (Mareuge and Lance 1995; Moghaddas et al. 2002). In the present study, the PLIF technique has been adapted to the specific case of a two-dimensional bubble swarm. Two fluorescent dyes and two cameras have been combined to fix the problems induced by the temporal and spatial fluctuations of the incident light and by the multiple light reflections at the bubble interfaces. We first describe the experimental conditions and the specific PLIF technique used. Then, we present and discuss original results concerning the mixing mechanisms of a passive scalar in the bubble swarm.

2 Experimental set-up and instrumentation

2.1 Experimental configuration

The experimental cell is made of two vertical glass plates of 800×400 mm^2, separated by a gap $w = 1$ mm (Fig. 1). The cell is filled with an aqueous solution of magnesium sulphate ($MgSO_4$) at 0.05 mol L^{-1}. The use of this very low concentrated electrolyte avoids bubble coalescences by introducing short-range nonhydrodynamic repulsion forces between gas–liquid interfaces, without changing significantly the physical properties of distilled water (Tsao and Koch 1994). This leads to a monodisperse swarm of bubbles. The liquid is initially at rest, and bubbles are produced at the bottom of the cell by injection of air through a set of 16 capillary tubes of 0.6 mm inner diameter equally distributed all over the base of the cell in order to avoid large-scale recirculation of liquid. The tubes are connected to an air reservoir the volume of which is large ensuring a stationary gas flow rate. The gas volume fraction α is varied from 1.3 to 7.5 %, by adjusting the air flow injected into the reservoir. The average equivalent diameter d of the bubbles evolves within 3.9 and 4.2 mm as α increases. For each values of α, d is large enough compared to the gap to ensure that $w/d < 1$, i.e. the bubbles are flattened due to the confinement (Fig. 1). The Reynolds number $Re = \rho\, V_0\, d/\mu$ evolves slightly between 450 and 500 while the Weber number $We = \rho\, V_0^2\, d/\sigma$ remains close to 0.7. Here, ρ, μ and σ are the density, dynamic viscosity and surface tension of the liquid phase, respectively, and V_0 is the rising velocity of a single bubble, which scales as $0.57\sqrt{gd}$. It is worth noting that the flow is dominated by inertia, since both Re and $Re(w/d)^2$ are high, and thus differs from the classical Hele-Shaw regime.

The mixing experiment consists in injecting a fluorescent dye during 3 s, at a given flow rate, through a capillary tube of inner diameter 0.6 mm immersed within the bubble swarm and connected to a controlled syringe. We record the temporal evolution of the global mass of dye, $M(t)$, observed in a given window. The measurement window is a rectangle of area $S = 115 \times 70$ mm^2, located 5 mm above the tip of the capillary tube. The location of the

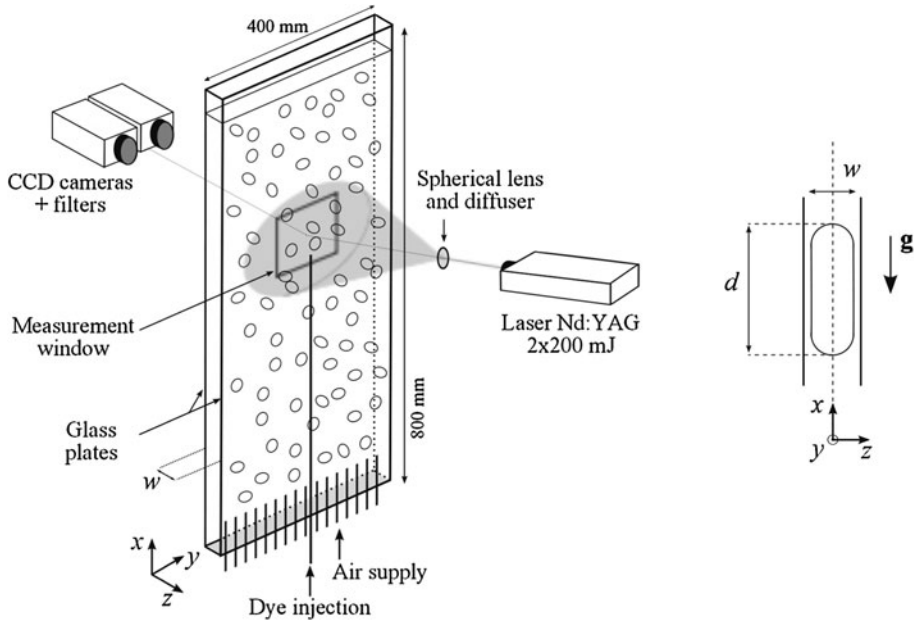

Fig. 1 (*left*) Experimental set-up (bubbles are not to *scale*). (*Right*) Side view of a bubble rising within the cell gap

measurement window is chosen 450 mm far from the bubble injection zone to ensure that the gas volume fraction and the bubble velocities profiles are flat meaning that the bubbly flow remains uniform and not affected by the presence of the thin capillary. We have performed two series of injections, one with an injection velocity of dye of 2.2 cm s^{-1} and the other with 5.3 cm s^{-1}, in order to check that the evolution of the normalized mass does not depend on the injected mass. At least 6 acquisitions lasting 10–20 s have been done for each of the investigated gas volume fractions ($\alpha = 1.3$, 3.2 and 7.5 %), which have shown a satisfactory reproducibility. After the end of the injection, the dye is transported only by liquid motions induced by the bubbles. It has been checked from PIV measurements that the average liquid velocity $\langle U \rangle$ is zero everywhere in the swarm. The evolution of $M(t)$ is related by a simple mass balance to the flux of mass, denoted $\mathbf{\Psi}$, at the frontiers Γ of this region.

$$\frac{\mathrm{dM(t)}}{\mathrm{d}t} = \oint_{\Gamma} \mathbf{\Psi} \cdot \mathbf{n} \mathrm{d}S \tag{1}$$

Even if the analysis is based on this integral description, where local fluxes are not directly measured, it gives access to new and valuable insights. Indeed, these measurements allow us to test whether a Fickian closure law for the mass transport is valid or not to model the effect of the bubble-induced agitation on the mixing.

2.2 Two-dyes PLIF technique

The in-plane concentration of the fluorescent tracer is measured by exciting the injected dye using a Nd:YAG pulsed laser (Quantel bi-pulse 2 × 200 mJ, $\lambda = 532$ nm, 10 Hz), and recording the fluorescence emission. An array of spherical micro-lenses used as a diffuser is coupled with a spherical lens and both cross the excitation light path. This optical device makes the laser beam divergent, providing thus a volume illumination of the cell (Fig. 1). The depth of field is larger than the width of the gap so that the in-plane concentration measurements are averaged over the gap of the cell. Here, the concentration of dye is expected to be uniform through the gap because the bubble-induced liquid motions are in-plane motions. The volume illumination technique, already implemented to measure rapid variations of the flow around a single bubble rising in the same experimental conditions, has been proved to give reliable measurements of the liquid in-plane velocities averaged through the cell gap (Roudet et al. 2011). The main concern with PLIF measurements is the determination of the relation between the fluorescence intensity I_f and the concentration of the fluorescent tracer C_f at a given location of the field of view. The general expression is as follows :

$$I_\mathrm{f} = I_\mathrm{Laser} A \Phi_\mathrm{q} w \epsilon C_\mathrm{f} = I_\mathrm{Laser} k_\mathrm{f} C_\mathrm{f} \tag{2}$$

where A is the fraction of the fluorescence light collected, Φ_q is the quantum efficiency of the tracer, ϵ its molar absorptivity. The fluorescence intensity depends also on the excitation laser light I_Laser. In classic PLIF measurements, the relation (2) is linear for low tracer concentration range, and the value of k_f, related to both the set-up and the dye properties, can be deduced from a calibration curve by assuming that I_Laser is constant over the measurement window. Here, the array of micro-lenses causes spatial patterns in the excitation intensity field, the amplitude of

which may correspond to 8 % of the light intensity averaged over the whole measurement window (Fig. 2a, b). The excitation light may also fluctuate in time by 10 % (±5 %) during the duration of an acquisition (Fig. 2a, c). In bubbly flows, an additional complexity comes from the light scattering and from the reflections at the bubble interfaces that sometimes focus the excitation light in the measurement window (Fig. 3).

These optical problems induce both temporal and spatial fluctuations of the excitation light that generate fluctuations of the captured light intensity that are superimposed to the effective fluorescence signal of the injected dye, making irrelevant the use of a standard PLIF procedure. To avoid these drawbacks, the fluctuating defects of the excitation light as well as the total fluorescence signal must be recorded simultaneously in order to perform both spatial and temporal corrections and determine the effective fluorescence signal, which is proportional to the concentration of the fluorescent

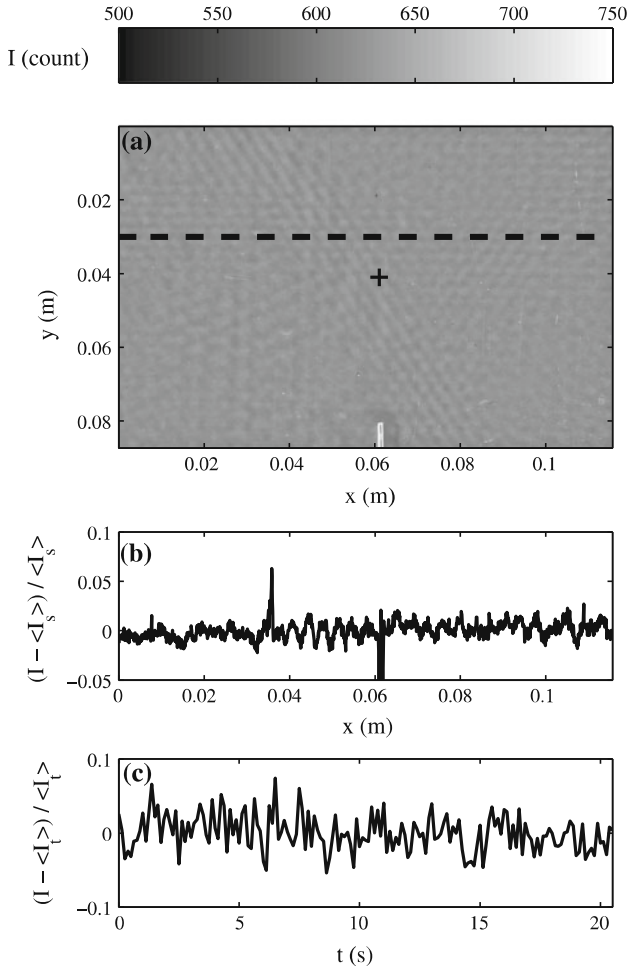

Fig. 2 **a** Fluorescence intensity field without any dye injection. **b** Spatial evolution of the intensity along the *dashed line* in **a**. **c** Temporal evolution of the intensity at the point + over 20 s, which is the duration of an acquisition

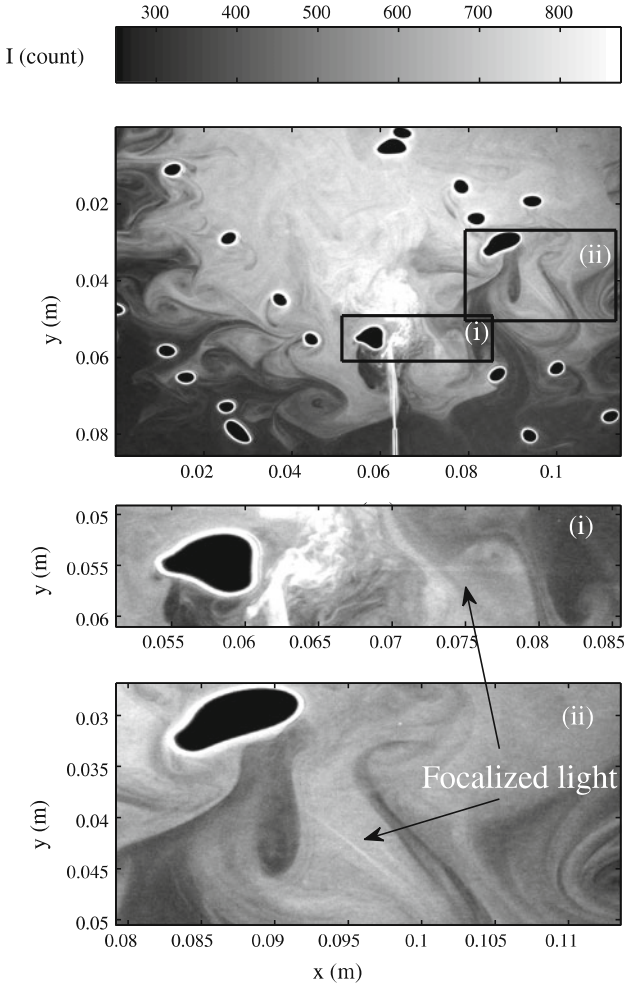

Fig. 3 Focalizations of the incident laser light at the interfaces of the bubbles. Here, two thin beams of focalized light can be seen in the two *black boxes* that are zoomed in *i* and *ii*. Bubbles are in *black*

tracer we want to track. We used thus a two-dyes PLIF technique with two fluorescent dyes of low molecular diffusivity (Table 1): Rhodamine WT ($C_{29}H_{29}N_2O_5ClNa_2$) and fluorescein sodium ($C_{20}H_{10}O_5Na_2$). The absorption and emission spectra of these dyes were measured using a spectrophotometer (Thermo, Heλios γ, Electron Corporation) and a spectrometer (Ocean Optics, USB 2000-FL), respectively. The corresponding spectra are shown in Fig. 4.

Rhodamine WT is added as a first fluorescent dye to the aqueous solution of magnesium sulphate in order to achieve a homogeneous concentration $C_{\text{rhoda}} = 5 \times 10^{-6}$ mol L^{-1}, which is kept constant during all the experiments. When exited at 532 nm, the rhodamine that is present in the liquid generates the fluorescence of the fluctuating background at a wavelength above 500 nm, even if no dye injection occurs. Fluorescein is the fluorescent tracer of which we want to measure the concentration. The solution injected through the capillary tube is

Table 1 Properties of the two fluorescent dyes used for concentration measurements

Fluorescent dye	Molecular formula	Molecular diffusivity D_{dye} ($cm^2\ s^{-1}$)	CAS	Provider
Rhodamine WT	$C_{29}H_{29}N_2O_5\ ClNa_2$	2.3×10^{-6}	37299-86-8	Cole-Parmer
Fluorescein sodium	$C_{20}H_{10}O_5Na_2$	5.1×10^{-6}	518-47-8	Fischer Scientific

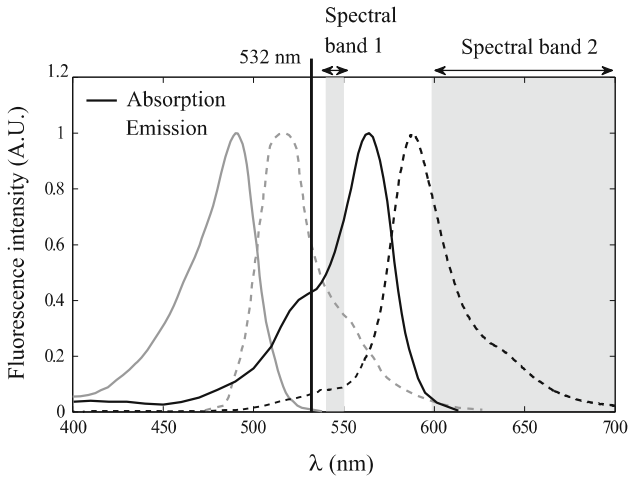

Fig. 4 Absorption and emission spectra of Fluorescein Sodium (*grey*) and Rhodamine WT (*black*). The wavelength of the laser light is 532 nm, and the fluorescence emission is collected in two different spectral bands, one for each of the two cameras

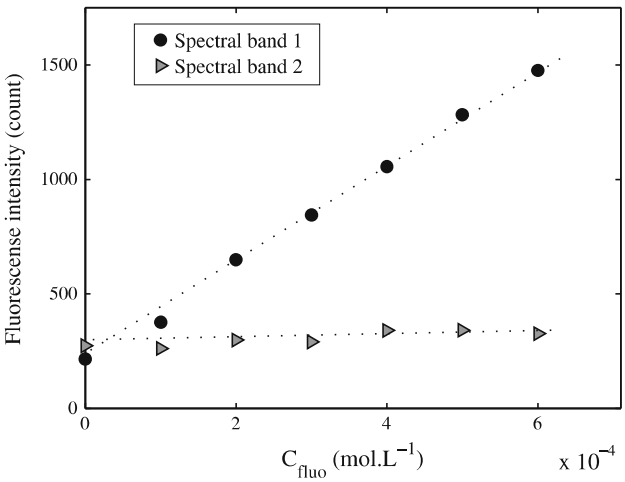

Fig. 5 Evolution of the fluorescence intensity measured in each spectral band as a function of fluorescein concentration, the concentration of rhodamine remaining equal to 5×10^{-6}mol L^{-1}

the same as the one present in the cell wherein fluorescein has been added to obtain a volume concentration $C_{fluo} = 5 \times 10^{-4}$ mol L^{-1}. Note that there is a significant overlap between the emission spectrum of the fluorescein and the absorption spectrum of the rhodamine. The fluorescence light emitted by the fluorescein can thus excite the rhodamine, this point will be addressed later.

Fluorescence emission is recorded on two synchronized CCD cameras (PCO sensicam QE, 1,376 × 1,040 pixels, 12 bits). Measurements are performed in complete dark conditions at 8 frames per second (Fig. 1), and the shutter speed of the cameras is 2 ms, making the exposure of the CCD sensors controlled by the duration of the laser pulses (10 ns). Both cameras are equipped with a 105 mm Nikkor lens carrying high-pass optical filter with a cut-off wavelength of 540 nm in order to filter the incident laser light. Each camera records light in its specific spectral band (Fig. 4). Camera 1 is used to record the concentration of the fluorescein. It is equipped with a low-pass filter with a cut-off wavelength of 550 nm (Melles Griot 03 SWP 608) and captures light in the spectral band 1 [540, 550 nm] (Fig. 4). It records the whole fluorescence signal I_{f1}, including the fluorescence of the fluctuating background (Fig. 3). Camera 2 is used to record the fluctuating background. It carries a high-pass filter with a cut-off wavelength above 600 nm (Hoya HMC R[25A]). Above 600 nm, the emission of the fluorescein is very weak, and the fluorescence emission I_{f2} recorded in spectral band 2 mainly corresponds to the fluorescence of the Rhodamine WT.

A calibration was performed separately in each spectral band by measuring the average fluorescence intensity field recorded simultaneously by the two cameras during 20 s, which is the standard duration of our acquisitions. The calibration was done in the same temperature and pH-controlled environment as for our acquisitions but without any injection nor bubble, and the intensity was averaged in space all over the measurement window and in time over 165 images, in order to get rid of fluctuating defects. The homogeneous concentration of Rhodamine WT in the cell was kept constant, whereas the homogeneous concentration in fluorescein C_{fluo} was increased from 0 to 6×10^{-4} mol L^{-1} (Fig. 5). For each calibration point, the solution in the cell was entirely renewed and we checked that no photobleaching of the two fluorophores occurred during the duration of an acquisition. Figure 5 shows the linear increase of fluorescence emission in the first spectral band as the concentration C_{fluo} increases, confirming that spectral band 1 is mainly sensitive to the fluorescein emission. Note, however, that there is a nonzero intensity I_{01} measured when C_{fluo} equals 0. This offset could be explained by a slight residual level of emission of Rhodamine WT in the considered spectral band. The fluorescence intensity measured in spectral band 2 keeps a constant value I_{02} whatever C_{fluo} and can thus be used as a normalizing signal. Note that the possible excitation of the Rhodamine WT

by the fluorescence emission of the fluorescein mentioned above is here confirmed to be negligible. Otherwise, the intensity measured in spectral band 2 should have increased with increasing C_{fluo}. Calculating the fluorescence intensity ratio for each pixel in the two spectral bands yields:

$$\frac{I_1}{I_2} = \frac{I_{f1} - I_{01}}{I_{f2} - I_{02}} = \frac{k_1}{k_2 C_{\text{rhoda}}} C_{\text{fluo}} \tag{3}$$

It does not depend any longer on the fluctuating excitation light since I_{Laser} is the same for each pixel in the two spectral bands. I_{01}, I_{02} and k_1/k_2 C_{rhoda} the constant slope of the curve of the intensity ratio are measured or known from calibration, and C_{fluo} can be derived from Eq. (3).

2.3 Image registration procedure and mass measurement

In our experiments, we used two independent cameras with their own optics (Fig. 1). Their optical axes are slightly different so that they image the same field from slightly different points of view (Fig. 1). Before calculating the ratio of the intensities measured in the two spectral bands to deduce the in-plane concentration of fluorescein, we must ensure that the reference image from camera 2 is perfectly mapped to the picture of camera 1. In other words, we must find the geometric transformation that match each point of coordinates (x_{i2},y_{i2}) imaged from camera 2 to its corresponding point of coordinates (x_{i1},y_{i1}) on the image from camera 1. This operation is done directly by finding characteristic points on the pictures from the two cameras viewing the same bubbles. The image registration is done using Matlab software. The first step consists in the detection of all the bubbles on both images. Only entire bubbles that do not intersect the images edges are selected, and each bubble detected on the image from camera 2 is labelized and matched with its corresponding bubble on the image from camera 1. We then perform a perspective correction by determining a geometrical transformation, based on four characteristic points of known coordinates, to find the projective transformation used to map image 2 to image 1. The new coordinates of image 2 in the frame of image 1 are calculated doing a bicubic interpolation, and a median filter was applied to image 2 before normalization to reduce the effect of the readout noise from the CCD sensor of camera 2. The two images are eventually cropped on the common zone, and the normalized image results from pixel-to-pixel ratio of the two images after their respective offsets have been removed. Note that the image registration is here done on bubbles themselves, as the four characteristic points are bubbles centroids. They were chosen near the corners to increase the precision of the image transformation algorithm. An estimation of the reliability of our image registration procedure has shown that the error on the new coordinates of image 2 does not exceed 0.3 pixel.

The image registration procedure was applied to each record (165 images, 8 Hz). The normalization of the total fluorescence signal with the reference signal allowed to discard the optical problems mentioned in Sect. 2.2: as an example, Fig. 6 illustrates the correction of the nonuniformities of the incident laser light. Then, the evolution of the concentration field $C_{\text{fluo}}(x, y, t)$ is obtained from Eq. (3), and the mass field of fluorescein is eventually calculated as

$$m(x, y, t) = \frac{I_1}{I_2}\frac{k_2}{k_1} C_{\text{rhoda}} w \Delta x^2 M_{\text{Fluo}} \tag{4}$$

and shown in Fig. 7. In Eq. (4), Δx is the pixel size, equal to 8.4×10^{-5}m and M_{Fluo}, the molecular weight of Fluorescein Sodium ($M_{\text{Fluo}} = 376.28$ g mol^{-1}).

3 Results and discussion

3.1 Mechanisms involved in the mixing

The agitation in the liquid phase has been investigated by a PIV method specially developed for the flow in the Hele-Shaw cell (Roudet et al. 2011). An instantaneous velocity field in the liquid phase is shown in Fig. 8. It reveals the major basic features of this original agitation that have been carefully characterized (Bouche et al. 2010). For the present purpose, we recall that (1) the agitation in the liquid results from wake interactions (in Fig. 8, when bubbles are

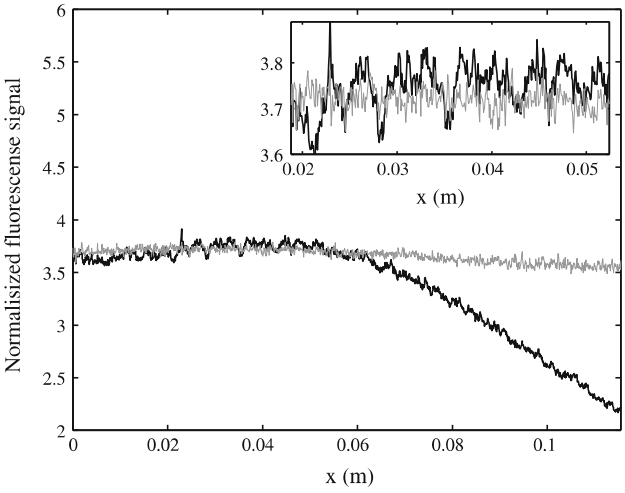

Fig. 6 Horizontal profiles of the normalized fluorescence signal from an image without bubbles: raw profile from camera 1 (*black line*) and profile of the intensity ratio I_1/I_2 given from Eq. (3) (*grey line*). *Inset* zoom where the spatial fluctuations due to the array of micro-lenses are shown to be significantly decreased. Note that for sake of clarity, the two profiles are displayed on the same graph

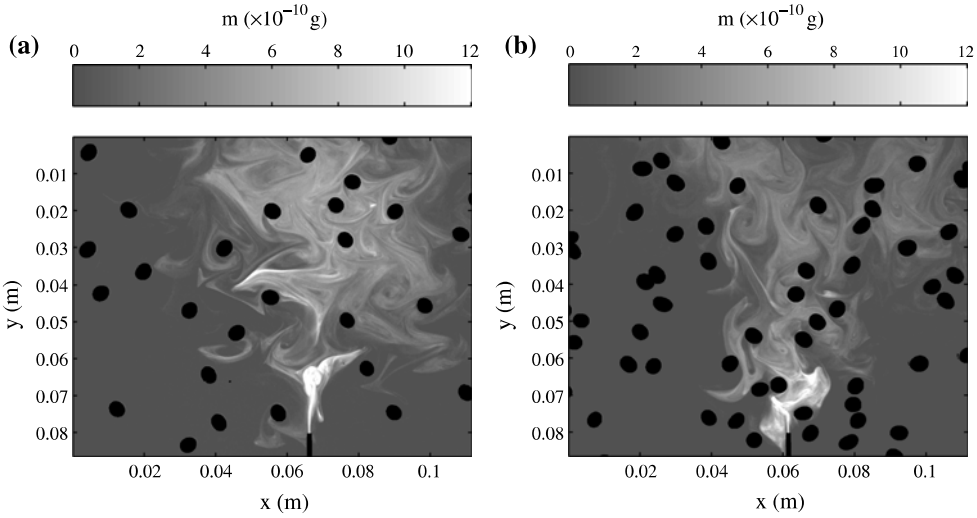

Fig. 7 Instantaneous mass distribution of fluorescein in a swarm at $\alpha = 3.2$ % (**a**) and $\alpha = 7.5$ % (**b**), near the end of dye injection

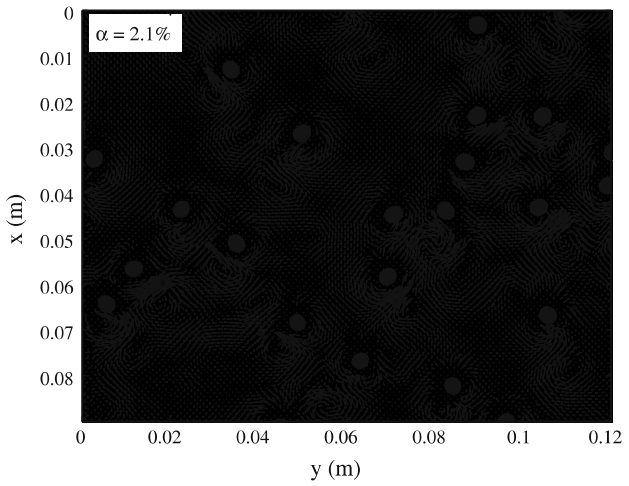

Fig. 8 Instantaneous velocity field in the liquid phase for $\alpha = 2.1$ % (the maximum vector size is similar to the velocity of the bubbles). The velocities in the liquid phase are due to the bubbles and fall to zero far from the bubbles

far from their neighbours, trailing vortices that decrease rapidly due to the shear stress at the walls can be identified, when bubbles are close together collective wake interactions become apparent); (2) the velocity fluctuations are quite isotropic due to the major contribution of the released vortices as compared to the contribution of entrainment of liquid in the mean wakes; (3) various length scales participate to the energy spectrum, the largest that can be identified in Fig. 7 being of about $5d$; and finally, (4) there exist regions of liquid with no motion at all due to the strong damping of the liquid motions by the confinement.

Instantaneous spatial distributions of dye are shown in Fig. 7 for two gas volume fractions at the end of injection. Far from the injector, both mass fields are characterized by thin and stretched lamellar structures, which are curved by the velocity field in the vicinity of the bubbles. The signature of the transport in the vortices of the wake is visible, as well as the distortion of the mass filaments in the potential flow just upstream of the bubbles. One can notice that in the regions where there is no bubble, the liquid is expected to be at rest due to the damping of its motion by the walls. Therefore, the inhomogeneous field of mass is, there, the result of the deposit of dye by the bubbles that passed through this region before.

3.2 Temporal evolution of the mass

The exponential decrease of $M(t)$ is shown on Fig. 9, where the normalized mass of dye has been plotted as a function of time in semi-logarithmic coordinates. An important result of this study is that, for large enough time, the mass of dye within the measurement window follows an exponential temporal decrease:

$$M(t) \sim M_{\max}\, \mathrm{e}^{\frac{-(t-t_0)}{\tau_m}} \tag{5}$$

with $M_{\max}$ the maximum value of the mass present in the measurement window after injection and τ_m the characteristic time of mixing. The time origin corresponds to the beginning of the injection, which lasts 3 s. The instant t_0 when the maximum is reached in all cases close to 4 s, which corresponds to 1 s after the end of injection. This time interval is of the order of the viscous time τ necessary for any agitation induced by the injection system to be dampened. Therefore, from t_0, the transport of dye is achieved by random bubble-induced motions as illustrated in Fig. 8. The time scale of mixing τ_m decreases when the gas volume fraction is increased, which shows that the efficiency of the mixing is enhanced in dense bubble swarms (Table 2).

The temporal evolution of a mass $M(t)$ of dye over the measurement window of area S is related to its concentration $C(x, y, t)$ and to its molecular weigh M_{dye}

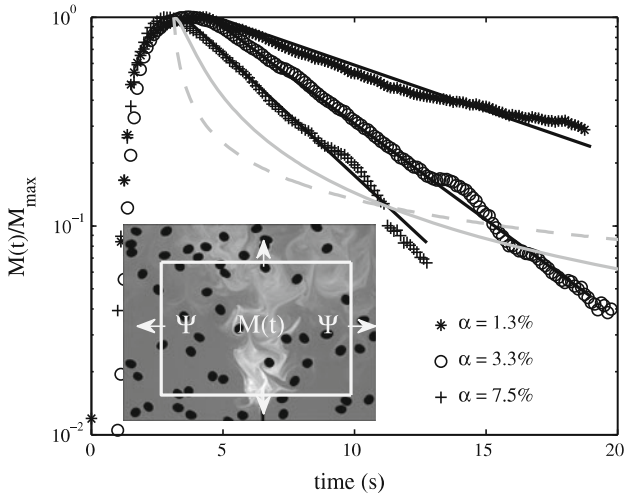

Fig. 9 Time evolution of the normalized mass of dye measured by PLIF for three different gas volume fractions. The black lines are exponential fits of the experimental data, and the grey lines are the predictions assuming a Fickian diffusion (*dashed line* 1D diffusion of a mass of dye initially located on a line; *plain line* isotropic diffusion of an initial Dirac distribution). *Inset* instantaneous mass distribution in the measurement window

Table 2 Evolution of the characteristic time scale for mixing τ_m with the gas volume fraction

α (%)	1.3	3.3	7.5
τ_m (s)	10	4.7	3.7

by:Assuming a Fickian diffusion of an initial patch of dye located on a horizontal line and transported in the vertical direction y, the temporal evol

$$M(t) = w\Delta x^2 M_{\text{dye}} \int\int_S C(x,y,t)\mathrm{d}x\mathrm{d}y. \quad (6)$$

ution of the mass $M(t)$ of dye is related to the concentration

$$C(x,y,t) = \frac{1}{2\sqrt{\pi D t}} \mathrm{e}^{\frac{-y^2}{4Dt}}, \quad (7)$$

where D is an effective diffusivity of the dye. The corresponding evolution of $M(t)$ is represented in Fig. 9 in grey dashed line. The value of the diffusivity has been chosen in order to match the experimental levels of $M(t)/M_{\max}$ of about 0.1 at $t = 11$s. It is clearly not in agreement with the experiments. The isotropic diffusion of a Dirac distribution initially located at the centre of the window leads to a concentration field

$$C(x,y,t) = \frac{1}{2Dt} \mathrm{e}^{\frac{-(x^2+y^2)}{4Dt}}, \quad (8)$$

The corresponding evolution of mass obtained with a diffusivity chosen to relax to similar levels is plotted in grey line in Fig. 9. Again, it is not in agreement with the experiments. It can therefore be concluded that the mixing in the confined bubble swarm cannot be reproduced by a Fickian law of diffusion. The mechanisms of mixing by bubbles in confined geometry are original and unexpected.

4 Conclusion

A two-dyes PLIF technique has been adapted to perform in-plane mass measurements in a confined bubbly flow. A laser is used to illuminate the gap of a Hele-Shaw cell. Measurement disturbances caused by light reflections at bubble interfaces were removed using two fluorescent dyes. Thanks to this technique, the time evolutions of concentration fields of a passive scalar dissolved within the liquid have been measured. These evolutions reveal the mechanisms responsible of the mixing in a confined bubbly swarm. Each bubble captures a certain amount of dye in its wake, transports it along a given distance and eventually releases it. The time evolution of the total amount of dye within a given window of observation has been shown to decay exponentially, which is not compatible with a Fickian diffusion process. The exponential time scale is a decreasing function of the gas volume fraction. The convective and intermittent character of the mixing is responsible for this peculiar behaviour. In the context of confined bubbly flows, future work will be devoted to the development of a mixing model accounting for the transport by the bubbles.

Similar experiments in three-dimensional bubble columns should allow to determine whether the bubble-induced mixing is similar in unconfined geometry. This requires to extend the present fluorescent technique to deal with situations where bubbles can hide each other and intercept the laser light.

Acknowledgments This work was supported by CNRS and the lab federation FERMaT.

References

Abbas M, Billet AM, Roig V (2009) Experiments on mass transfer and mixing in a homogeneous bubbly flow. 6th International symposium on Turbulence, Heat and Mass Transfer, Sept 14–18, Rome, Italy

Besnaci C, Roig V, Risso F (2010) Mixing induced by a random dispersion at high particulate Reynolds number. In: International conference on multiphase flows, Tampa

Bouche E, Billet AM, Roig V, Risso F (2010) Agitation in a swarm of confined bubbles. In: 8th European fluid mechanics conference EFMC8, Bad Reichenhall, Germany

Bouche E, Roig V, Risso F, Billet AM (2012) Homogeneous swarm of high-Reynolds-number bubbles rising within a thin gap. Part 1: Bubble dynamics. J Fluid Mech 704:211–231

Coppeta J, Rogers C (1998) Dual emission laser induced fluorescence for direct planar scalar behaviour measurements. Exp Fluids 25:1–15

Crimaldi JP (2008) Planar laser induced fluorescence in aqueous flows. Exp Fluids 44:851–863

Eames I, Bush JWM (1998) Longitudinal dispersion by bodies fixed in a potential flow. Proc R Soc Lond A 455:3665–3686

François J, Dietrich N, Guiraud P, Cockx A (2011) Direct measurement of mass transfer around a single bubble by micro-PLIFI. Chem Eng Sci 66:3328–3338

Mareuge I, Lance M (1995) Bubble induced dispersion of a passive scalar in bubbly flows. Int Conf on Multiphase Flows, Kyoto

Moghaddas JS, Trägårdh C, Kovacs T, Östergren K (2002) A new method for measuring concentration of a fluorescent tracer in bubbly gas-liquid flows. Exp Fluids 32:728–729

Roig V, Roudet M, Risso F, Billet AM (2012) Dynamics of a high-Reynolds-number bubble rising within a thin gap. J Fluid Mech 707:444–466

Roudet M (2008) Hydrodynamique et transfert de masse autour d'une bulle confine entre deux plaques. PhD thesis, INP Toulouse, France

Roudet M, Billet AM, Risso F, Roig V (2011) PIV with volume lighting in a narrow cell: An efficient method to measure large velocity fields of rapidly varying flows. Exp Therm Fluid Sci 35:1030–1037

Soltys MA, Crimaldi JP (2011) Scalar interactions between parallel jets measured using a two-channel PLIF technique. Exp Fluids 50:1625–1632

Sakakibara J, Adrian RJ (1999) Whole field measurement of temperature in water using two-color laser induced fluorescence. Exp Fluids 26:7–15

Stöhr M, Schanze J, Khalili A (2009) Visualization of gas/liquid mass transfer and wake structure of rising bubbles using pH-sensitive PLIF. Exp Fluids 47:135–143

Tsao HK, Koch DL (1994) Collisions of slightly deformable, high Reynolds number bubbles with short-range repulsive forces. Phys Fluids 6:2591–2625